

Synthesis and Application of Surface-modified NiFe Nanoparticles as a new Magnetic Nano Adsorbent for the Removal of Nickel Ion from Aqueous Solution

Y.Liu, P. F. Dai, X. W. Li and Y. Zhu

School of Metallurgy, Northeastern University, Shenyang 110819, China
(E-mail: liuy@smm.neu.edu.cn)

Abstract

Magnetic alloy Ni_{2.33}Fe nanoparticles were prepared using hydrothermal method and used for removing nickel ion from aqueous solution. The magnetic particles were characterized by XRD, SEM, TG and FTIR, which confirms that the magnetic product is nano NiFe alloy with fcc-type structure and its surface were successfully modified by sodium citrate. The adsorption kinetics studies were performed and pseudo-second-order kinetic model successfully described the kinetic data. The Freundlich and Langmuir adsorption models were used for the mathematical description of adsorption equilibrium and it was found that the experimental data fitted very well to the Freundlich model.

Keywords

Adsorption; Freundlich adsorption model; kinetics; magnetic alloy particles; nickel ion

INTRODUCTION

A growing number of heavy metals are generated among a wide range of industries (mining, metal processing, electroplating, electronics, etc.). It is necessary to move these heavy metal ions before being discharged to water systems, or these heavy metal ions could enter the food chain through drinking water and crop irrigation to lead to a risk to human beings [Peng et al., 2004]. Thus, how to effectively and deeply remove them from water system is still a very important but still challenging task. People are increasingly interested in studying different approaches to removal them from waste water.

Nowadays, some approaches have been developed and used to remove hazardous pollutants from wastewaters, such as coagulation/flocculation [Ahammed et al 2014], chemical precipitation [Zhu et al 2007], membrane filtration [Zheng et al 2013], catalytic and photocatalytic oxidation [Copper et al 1999; Larachi et al 2001], chlorination [Sinkkonen et al 1997], reverse osmosis [Arzuada et al 2008] and adsorption [Anbia & Lashgari 2010]. Among all of these techniques, adsorption is one of the widest applications in recent years because of simple, effective and low-cost.

Some traditional adsorbents, such as activated carbon [Guo et al 2010], Chitosan [Borsagli et al. 2015], zeolites [Nezamzadeh-Ejhih and Kabiri-Samani 2013], clays [Kaur et al 2015] and so on, have been used due to the relatively low price and wide sources. But a relatively low adsorbing efficiency becomes a limit to the utilization of these types of adsorbents. With the development of the technology, various nanomaterials have been reported to be used as adsorbents based on their extremely small size and high surface-area-to volume ratio [Hua et al 2011]. For example, [Afkhami et al 2010] developed 2,4-dinitrophenylhydrazine modified γ -Al₂O₃ for removal of metal cations Pb²⁺, Cd²⁺, Cr³⁺, Co²⁺, Ni²⁺ and Mn²⁺, the adsorption capacity of Ni²⁺ was 18.18 mg/g; [Tarasevich and Klimova 2001] also synthesized modified γ -Al₂O₃, the adsorption capacity of Ni²⁺ was 176.1 mg/g. Then again, amino-functionalized silica nano hollow sphere and silica gel [Najafi et al 2011], nano-calcium titanate [Zhang et al 2011], nano manganese dioxide [Fan et al 2005; Su

et al 2010], nanosized titanium oxides [Engates and Shipley 2011], nanosized magnesium oxides [Gao et al 2008], nanosized zinc oxides [Kikuchi et al 2006] and carbon nanotubes [Chen and Wang 2006] also been used as adsorbents and have demonstrated high adsorption efficiency for metal ion removal.

However, it will be more difficult to be separated from the water as the adsorbents are in nano-size. Hence, magnetic nanoparticles attract increasing attentions in comparison with other nano materials because they can use magnetic separation technology to improve the separation efficiency and reduce the separation cost during water/wastewater treatment [Ambashta and Sillanpää 2010]. The magnetic adsorbents that have been studied the most are ferric oxide [Gupta and Nayak 2012], ferrihydrite [Yuan et al 2010] and Fe [Boparai et al 2011]. They exhibit satisfactory adsorption capacity of toxic matters from aqueous solution (for example, the adsorption of capacities of Ni²⁺ was 23.6 mg/g [Hu et al 2006]).

In this study, a new surface-modified magnetic NiFe nano alloy particles were synthesized and characterized. It exhibits superior to iron oxides in oxidation resistance and more potential to be used repeatedly as magnetic adsorbents.

EXPERIMENTAL

Preparation of Ni_{2.33}Fe nanoparticles

The NiFe nanoparticles were synthesized using hydrothermal method [Liu et al. 2014]. Typically, 3:1 of molar ratio of dissoluble nickel salt to ferrous salt and a certain amount of sodium citrate was dissolved into specific volume of deionized water. Some volume of 1 M NaOH was added to the solution to adjust pH to around 12.5. Excess of hydrazine hydrate was dropped into the solution as reducing agent. The mixture solution was transferred to an autoclave after being stirred well under N₂. The autoclave was sealed and put into a furnace which was preheated to 120 °C. The autoclave was cooled to room temperature after heating for 19 h. NiFe nanoparticles were separated with magnetic bar from the solution. The products obtained were cleaned and re-dispersed in deionized water and ethanol several times.

Two different NiFe particles obtained by the above method were due to the dosage of sodium citrate. In the paper, the NiFe particle was prepared under the condition of the molar ratio of the total of Ni and Fe salts to sodium citrate of 1:10, another was that molar ratio of 1:0.2 [Liu et al 2014].

Characterization of the synthesized materials

X-ray diffraction(XRD) patterns were recorded on Rigaku D/MAX 2500 diffractometer. Scanning electron microscopy (SEM) was performed on Zeiss Ultra Plus model. Magnetization measurement(VSM) was using Lakeshore Model 7407 Vibrating Sample Magnetometer at room temperature. Thermogravimetric analysis (TG) was performed on TA Instruments SDT Q600. The infrared spectroscopy measurements (FT-IR) were performed on Perkin–Elmer Spectrum 100.

Adsorption experiments

For equilibrium experiment, 100 mg of Ni_{2.33}Fe nanoparticles was added into 30 mL of Ni²⁺ solution at a series of known initial concentrations (C₀). After stirring the samples for 24 h with an agitator, the magnetic particles were separated using a magnet from the solution.

The amount of the adsorbed pollutants to the magnetic adsorbents was calculated with Eq. (1)

$$q_e = \frac{(C_0 - C_e)}{m} \times V \quad (1)$$

For kinetic experiments, Zero time was taken when 200 mg of Ni_{2.33}Fe nanoparticles was added into 200 mL of Ni²⁺ solution with different initial concentrations. The solution was stirred and taken at appropriate time intervals.

RESULTS AND DISCUSSION

Characterization of adsorbent

The compositions of Ni and Fe in the as-synthesized NiFe nanoparticles were determined using ICP-OES method. The ratio of Ni to Fe is 2.33:1 in the paper, so the particle was expressed as Ni_{2.33}Fe. Another particle we reported from sodium citrate at 1:0.2 was Ni_{3.54}Fe [Liu et al 2014]. It demonstrated that the dosage of sodium citrate have significant impact on the compositions of the bimetallic particles.

The as-synthesized bimetallic particles were characterized by XRD, shown in Fig.1.

The two bimetallic particles have almost the same three peaks, which can be indexed to (111), (200) and (220) planes with face-centered cubic (fcc) type of structure. But a minor difference that can be seen from the two particles is subtle shift of 2θ. 2θ of (111) plane is 44.36° for Ni_{2.33}Fe, while it is 44.22° for Ni_{3.54}Fe [Liu et al 2014]. The structural parameters calculated based on peak positions of (111) plane of Ni_{2.33}Fe and Ni_{3.54}Fe are 3.536 nm and 3.533nm, respectively, which is in agreement with the fact that the atomic radius of iron is slightly larger than that of nickel and Fe–Fe bond length (2.7 Å) and Fe–Ni bond length (2.5 Å) are larger than that for Ni–Ni (2.14 Å) [Guirado-Lopez & Aguilera-Granja 2008]. It can be deduced that both Ni_{2.33}Fe and Ni_{3.54}Fe have the same basic structure of fcc type and are substitutional solid solution alloy of part of atoms of Ni substituted by atoms of Fe.

The particle sizes were calculated based on the peak width using Scherrer equation. The sizes values are 11.90 nm and 15.8 nm for Ni_{2.33}Fe and Ni_{3.54}Fe nanoparticles, respectively. It indicates the usage of sodium citrate can control the particle sizes of the bimetallic NiFe.

Fig, 2 shows the SEM image for the as-synthesized Ni_{2.33}Fe nanoparticles. There are two shapes of particles could be seen. The chainlike part (a part) showed that the diameter of chainlike wires is about 1 μm, and the length ranged from dozens to hundreds of microns, which the wires interconnected and the surface is aristate. Another shape is approximate sphere (b part), they were near-spherical, smooth, uneven and jointed. The atom compositions of the two parts from EDS were listed in Table 1. The contents of C, Ni and Fe in the two parts exhibited disparity.

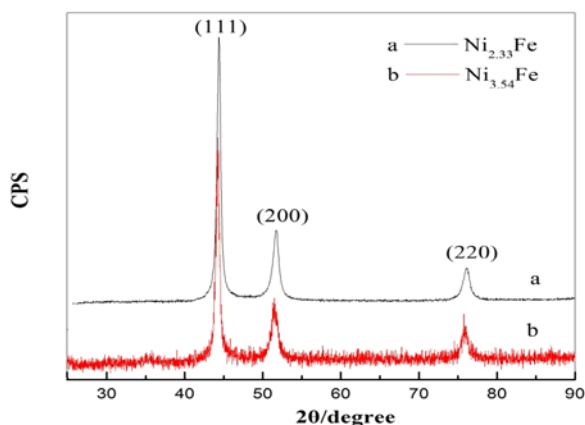


Figure 1. XRD patterns of samples (a) Ni_{2.33}Fe, (b) Ni_{3.54}Fe (a)

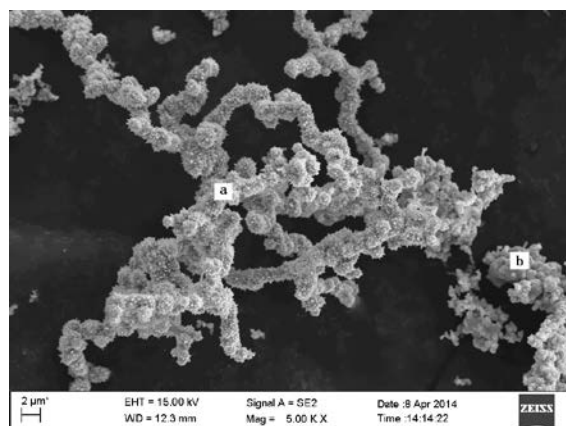


Figure 2. SEM images of Ni_{2.33}Fe nanoparticles

Table 1 the atom components at two positions from EDS

position	C (atom%)	Fe (atom%)	Ni (atom%)
a	52.17	5.70	42.14
b	67.66	6.76	25.59

The TG and DTA for the particles of Ni_{2.33}Fe and Ni_{3.54}Fe are shown in Fig.3. For Ni_{3.54}Fe, its baseline is flat below 400 °C, which it explains that there is no weight loss to happen in the temperature range. The further information deduced is likely that the surface of the Ni_{3.54}Fe particles does not adsorb volatile molecules, such as water or ethanol molecules. A sharp weight increase started at 400 °C, which originated from the oxidation of Fe and Ni at 450 °C and 656 °C (inset curve b). [Liu et al 2014].

An obvious difference for Ni_{2.33}Fe particles is that a weight loss of about 4.7% is observed below 400 °C, which the weight loss is due to the loss of the water or ethanol bound to Ni_{2.33}Fe particles. Same as Ni_{3.54}Fe particles, a sharp weight increase started at 400°C, but the weight increase come from the oxidation of Fe and Ni at 448 °C and 582 °C. Another difference appeared at 718 °C, Ni_{2.33}Fe particles exhibiting weight loss while Ni_{3.54}Fe particles showing weight increase. The weight loss of Ni_{2.33}Fe particles is attributed to the decomposition of citrate bound to the surface of the particles.

A further evidence about the existence of sodium citrate bound to the surface of Ni_{2.33}Fe particles was based on the characteristics of IR spectra. Comparison of the FTIR spectra of nano Ni_{3.54}Fe, nano Ni_{2.33}Fe and sodium citrate, it can be obviously seen from Fig.4 that there was a strong stretching vibration peak of C=O at 1623 cm⁻¹ in curve b, the same peak can be found in curve c, but the peak did not appear in curve a. The clear evidence shows that the surface of Ni_{2.33}Fe bound by sodium citrate, but Ni_{3.54}Fe did not.

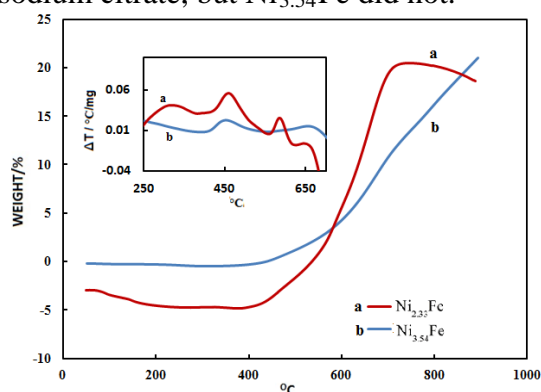


Figure 3. Thermogravimetric curves for nanoparticles synthesized from different citrate usages (a) Ni_{2.33}Fe, (b) Ni_{3.54}Fe

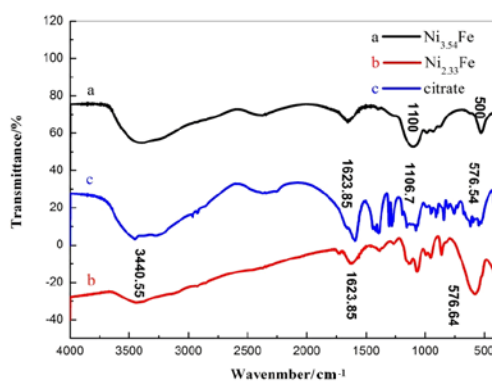


Figure 4. IR spectra of nano Ni_{3.54}Fe, nano Ni_{2.33}Fe and sodium citrate (a) Ni_{3.54}Fe, (b) Ni_{2.33}Fe, (c) citrate

The magnetic properties were characterized using vibrating sample magnetometer at room temperature. Fig.5 shows a representative set of magnetization curves for the particles of Ni_{3.54}Fe and Ni_{2.33}Fe. The magnetization hysteresis curves of two samples show S-shapes, characteristic of magnetically-soft materials. For Ni_{2.33}Fe, the values of the remanence (*M_r*), saturation magnetization (*M_s*) and coercivity (*H_c*) are 2.91 emu•g⁻¹, 75.44 emu•g⁻¹ and 45.9 Oe, they are 1.0 emu•g⁻¹, 56.3 emu•g⁻¹ and 14 Oe for Ni_{3.54}Fe, respectively.

Adsorption of Ni²⁺

Adsorption kinetics

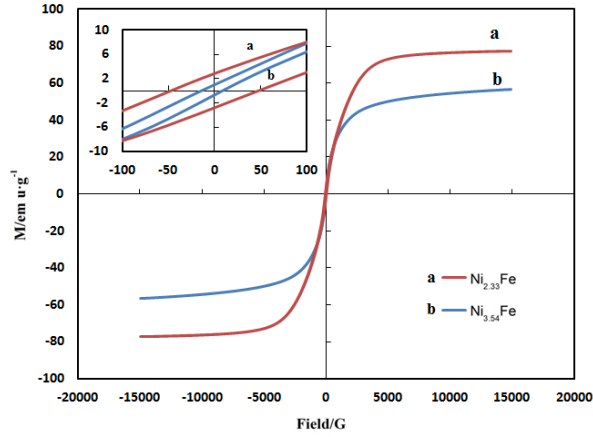


Figure 5. Magnetization curves for the nanoparticles synthesized from different citrate usages (a) $\text{Ni}_{2.33}\text{Fe}$, (b) $\text{Ni}_{3.54}\text{Fe}$

Lagergren's equation is the one most widely used for the adsorption of solute from a liquid solution. The pseudo-first-order kinetic equation may be written as

$$\log(q_e - q_t) = \log(q_e) - \frac{Kt}{2.303} \quad (2)$$

The pseudo-second-order equation is expressed as follows:

$$\frac{t}{q_t} = \frac{1}{k'q_e^2} + \frac{1}{q_e}t \quad (3)$$

where q_e and q_t (mg/g) are the amounts of Ni^{2+} adsorbed on $\text{Ni}_{2.33}\text{Fe}$ at equilibrium and at time t , respectively. K is the kinetic constant of pseudo-first-order adsorption (min^{-1}), and k' is the pseudo-second-order rate constant ($\text{g}/(\text{mg min})$).

If the second order kinetic equation fits the data well, q_e and k' can be determined through the slope and intercept of the plot because of a linear relationship of t/q_e against t of Eq. (3).

Adsorption dynamics of Ni^{2+} by nanomagnetic particles of $\text{Ni}_{2.33}\text{Fe}$ were investigated at different initial concentrations of Ni^{2+} and the results are shown in Figure. 6. It is clear that the q_t has rapid increase for contact time within 60 min, and sorption equilibration was achieved by 270 min, followed by a constant adsorption rate with further shaking time.

The values of $\log(q_e - q_t)$ were calculated from the kinetic data of Figure 6 and plotted versus t of Eq. (2). The adsorption parameters and the plots from pseudo-first-order kinetic model are presented in Table 1

It can be found the corresponding regression coefficients (R^2) based on the pseudo-first-order model within the whole adsorption is low ($R^2 < 0.85$), and the theoretical q_e values predicted by the pseudo-first-order model are very different to the experimental q_e values at different initial concentrations of Ni^{2+} .

Figure 7 shows the plots of the pseudo-second-order kinetic model for adsorption on magnetic nano- $\text{Ni}_{2.33}\text{Fe}$, where t/q_e is plotted against t . And adsorption kinetic parameters based on the pseudo-second-order equation (Eq.(3)) are presented in Table 2. The theoretical q_e values predicted by the pseudo-second-order model agree very closely to the experimental q_e values at different initial adsorbate concentrations. Further, a good linearity with R^2 above 0.999 also indicates the

adsorption kinetics follows the pseudo-second-order model.

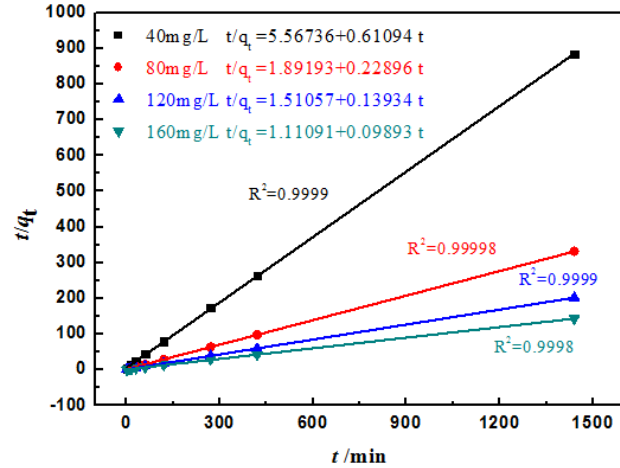
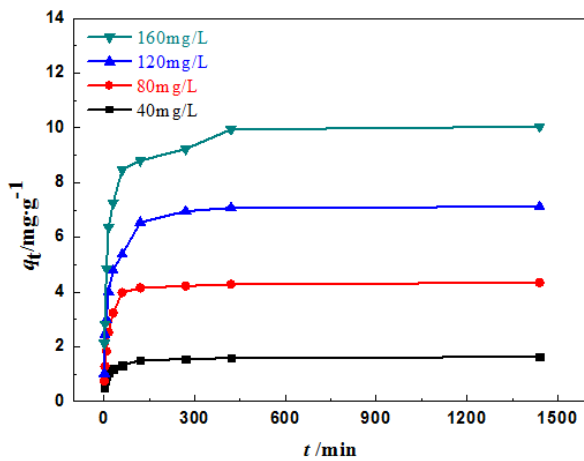


Figure 6. Ni²⁺ adsorption kinetics on magnetic Ni_{2.33}Fe nanoparticles at 20 °C; **Figure 7.** Plot of pseudo-second-order model at different concentrations of Ni²⁺ for Ni_{2.33}Fe as adsorbent initial Ni²⁺ concentrations: (a) 40 mg/l, (b) 80 mg/l, (c) 120 mg/l, (d) 160 mg/l

Table 2 Determined kinetic model constants for the adsorption of Ni²⁺ on Ni_{2.33}Fe at different initial concentrations

C ₀ (mg · L ⁻¹)	q _e (mg/g) exp.	Pseudo-first-order		q _e *	Pseudo-second-order		
		K(min ⁻¹)	R ²		K'(g/mg min)	R ²	q _e *
40	1.6295	0.00323	0.8245	0.468	0.06704	0.9998	1.6368
80	4.343	0.00312	0.6528	1.096	0.02771	0.9999	4.3676
120	7.117	0.00315	0.6584	2.135	0.01285	0.9999	7.1768
160	10.044	0.00314	0.7589	3.200	0.00881	0.9999	10.1082

Note: q_e* , (mg/g), calculated from pseudo-first-order model and pseudo-second-order model

Adsorption rate-controlling mechanism

The results obtained using the pseudo-second-order model are not enough to predict the diffusion mechanism [Akar et al., 2008]. Therefore, the intraparticle diffusion model is investigated to analyze the adsorption kinetic data.

The three steps involved in the adsorption of an organic/inorganic species by a porous adsorbent are as follows: (1) transport of the adsorbate to the external surface of the adsorbent (film-diffusion); (2) transport of the adsorbate within the pores of the adsorbent except for a small amount of adsorption that occurs on the external surface (particle diffusion); (3) adsorption of the adsorbate on the external surface of the adsorbent. The last step is considered to be fast enough, thus the slowest of the transport steps would determine the overall rate of adsorption. Intraparticle diffusion model based on the theory proposed by Weber and Morris was tested as

$$q_t = k_d t^{1/2} + C \quad (4)$$

where k_d (mg/g min^{1/2}) is the intraparticle diffusion rate constant, and C (mg/g) is a constant related to the thickness of the boundary layer. The plot of q_t versus $t^{1/2}$ gives a straight line and the straight line passes through the origin, then the sorption process is controlled by intraparticle diffusion only. However, if the data exhibit multi-linear plots, then the sorption process is controlled by two or more steps. The first sharper portion is the external surface adsorption or instantaneous adsorption stage. The second portion is the gradual adsorption stage, where the intraparticle diffusion is rate limited.

The diffusion model plots shown in Figure 8 are related by two straight lines during the adsorption process, indicating the adsorption was regulated by both surface and intraparticle diffusion processes. The first linear portion of the plot indicates boundary layer effect, i.e. surface adsorption while the second linear portion is due to the intraparticle diffusion. Moreover, all lines do not pass the original point. All these prove that intraparticle diffusion is not the only controlling factor. The slope of the second linear portion of the plot has been defined as a rate parameter (k_d), which characterizes the rate of adsorption in the region where pore diffusion is rate limiting. Thus all these suggest that in the adsorption of Ni^{2+} over the nano $\text{Ni}_{2.33}\text{Fe}$ was controlled by external mass transfer followed by intra particle diffusion mass transfer.

The values of K_{id} and C_i are listed in Table 2. It can be found that K_{i1} is larger than K_{i2} , while C_1 is smaller than C_2 , demonstrating that the global adsorption process is controlled by intraparticle diffusion.

Table 2

The intraparticle diffusion parameters for Ni^{2+} adsorption onto $\text{Ni}_{2.33}\text{Fe}$.

Initial concentration (mg L^{-1})	K_{i1} ($\text{mg g}^{-1} \text{min}^{1/2}$)	C_1	R^2	K_{i2}	C_2	R^2
40	0.113	0.533	0.922	0.0044	1.474	0.879
80	0.480	0.459	0.981	0.010	4.006	0.724
160	0.963	1.68	0.931	0.051	8.336	0.767

Adsorption isotherms

The Langmuir equation can be expressed as:

$$\frac{C_e}{q_e} = \frac{C_e}{q_m} + \frac{1}{q_m K_L} \quad (5)$$

where q_e is the equilibrium adsorption capacity of pollutants on the adsorbent (mg/g), C_e the equilibrium pollutant concentration in solution (mg/L), q_m the maximum capacity of adsorbent (mg/g), and K_L is the Langmuir adsorption constant (L/mg).

The linear form of Freundlich equation, which is an empirical equation used to describe heterogeneous adsorption systems, can be represented as follows:

$$\ln q_e = \ln K_F + \frac{1}{n} \ln C_e \quad (6)$$

where q_e and C_e are defined as above, K_F is Freundlich constant (L/mg), and n is the heterogeneity factor.

The values of q_m and K_L were determined from the slope and intercept of the linear plots of C_e/q_e versus C_e and of values of K_F and $1/n$ were determined from the slope and intercept of the linear plot of $\ln q_e$ versus $\ln C_e$.

The equilibrium adsorption capacities of Ni^{2+} are fitted by Langmuir and Freundlich isotherm equations (Eq.(5) and (6)), and the results of the data fitting are shown in Figure 9. In the Langmuir model, the regression coefficient, $R^2=0.8025$, is low, and slope of the linear is a negative value. It will get an unreasonable negative value of q_m . This implies that the Langmuir model could not represent the data reasonably well. The Langmuir describes monolayer adsorption and this means the monolayer adsorption is not suitable to the adsorbing of Ni^{2+} over $\text{Ni}_{2.33}\text{Fe}$.

The regression coefficient, R^2 , is 0.9923 based on the fitting the data on the Freundlich model. It

obviously fits better by Freundlich equation than by Langmuir equation. Thus, the adsorption of Ni^{2+} on the $\text{Ni}_{2.33}\text{Fe}$ obeyed the Freundlich adsorption isotherm. The values of K_F and $1/n$ were determined from the slope and intercept of the linear plot of $\ln q_e$ versus $\ln C_e$, they are 0.0177 and 1.1905, respectively. The value of $1/n$ between 1 and 2 indicates that Ni^{2+} can be adsorbed by the magnetic $\text{Ni}_{2.33}\text{Fe}$. Freundlich model, as an empirical model, is particularly suitable to describe the interaction of multi-layer ions and chemical adsorption.

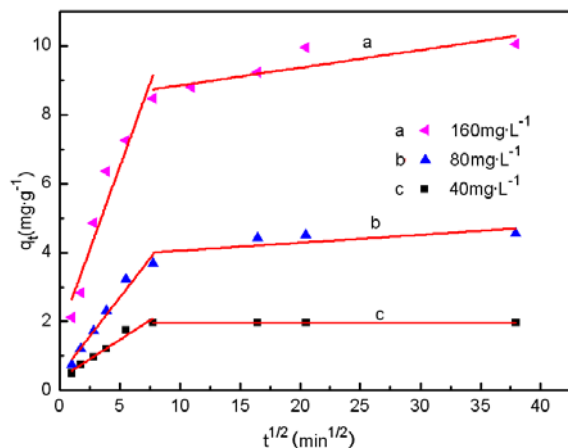


Figure 8. plot of Weber-Morris intraparticle diffusion model at different concentrations of Ni^{2+}

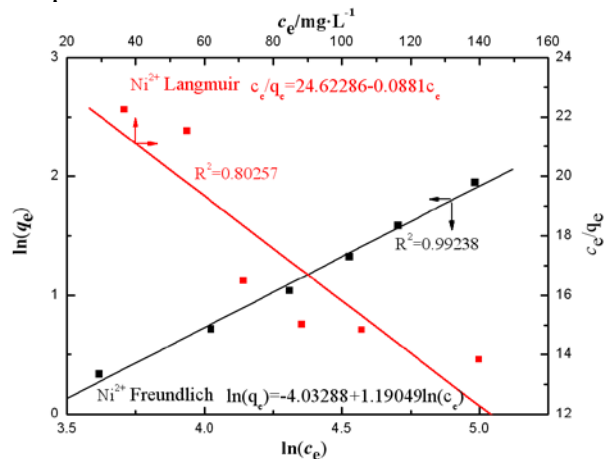


Figure 9. Adsorption isotherms of Ni^{2+} onto nano- $\text{Ni}_{2.33}\text{Fe}$ (a) Langmuir, (b) Freundlich

Acknowledgements

The research work was supported by National Natural Scientific Foundation of China 51574084

REFERENCES

- Afkhami, A., Saber-Tehrani, M., Bagheri, H. 2010 Simultaneous removal of heavy metal ions in wastewater samples using nano-alumina modified with 2,4- dinitrophenylhydrazine. *Journal of Hazardous Materials* 181, 836–844.
- Ahamed, S., Ajoy, S., Gajbhiye, V., Suman, G., Manjaiah, K., Eldho, V. 2014 Simultaneous removal of multiple pesticides from water: Effect of organically modified clays as coagulant aid and adsorbent in coagulation-flocculation process. *Environmental technology* 35(20), 2619-2627.
- Akar, T., Anilan B., Kaynak Z., Gorgulu A., Akar S. 2008 Batch and Dynamic Flow Biosorption Potential of *Agaricus bisporus/Thuja orientalis* Biomass Mixture for Decolorization of RR45 Dye. *Industrial and Engineering Chemistry Research* 47(23), 9715-9723.
- Ambashta, R., Sillanpää M., 2012. Water purification using magnetic assistance: A review. *Journal of Hazardous Materials* 180, 38–49.
- Anbia, M., Lashgari, M. 2010 Synthesis of amino-modified ordered mesoporous silica as a new nano sorbent for the removal of chlorophenols from aqueous media. *Chemical Engineering Journal* 150(2-3), 555-560.
- Arzuada, J., Lopez-Munoz, M., Aguado, J. 2008 Temperature, pH and concentration effects on retention and transport of organic pollutants across thin-film composite nanofiltration membranes. *Desalination* 221(1-3), 253–258.
- Boparai, H., Joseph, M., O'Carroll, D. 2011 Kinetics and thermodynamics of cadmium ion removal by adsorption onto nano zerovalent iron particles. *Journal of Hazardous Materials* 186, 458–465.

- Borsagli F., Mansur A., Chagas P., Oliveira L., Mansura H. 2015 O-carboxymethyl functionalization of chitosan: Complexation and adsorption of Cd (II) and Cr (VI) as heavy metal pollutant ions. *Reactive and Functional Polymers* 97, 37-47.
- Chen, C., Wang, X. 2006 Adsorption of Ni(II) from aqueous solution using oxidized multi-wall carbon nanotubes. *Industrial & Engineering Chemistry Research* 45, 9144–9149.
- Copper, C., Burch, R. 1999 An investigation of catalytic ozonation for the oxidation of halocarbons in drinking water preparation. *Water Research* 33(18), 3695–3700.
- Engates, K.E., Shipley, H.J. 2011 Adsorption of Pb, Cd, Cu, Zn, and Ni to titanium dioxide nanoparticles: effect of particle size, solid concentration, and exhaustion. *Environmental Science and Pollution Research* 18, 386–395.
- Fan, M., Boonfueng, T., Xu, Y., Axe, L., Tyson, T.A. 2005 Modeling Pb sorption to microporous amorphous oxides as discrete particles and coatings. *Journal of Colloid and Interface Science* 281, 39–48.
- Gao, C.L., Zhang, W.L., Li, H.B., Lang, L.M., Xu, Z. 2008 Controllable fabrication of mesoporous MgO with various morphologies and their absorption performance for toxic pollutants in water. *Crystal Growth & Design* 8, 3785–3790.
- Guo, M.X., Qiu, G.N., Song, W.P. 2010 Poultry litter-based activated carbon for removing heavy metal ions in water. *Waste Management* 30, 308-315.
- Guirado-Lopez, R. A., Aguilera-Granja, F. 2008 Bimetallic Fe-Ni cluster alloys: Stability of core(Fe)-shell(Ni) arrays and their role played in the structure and magnetic behavior. *Journal of Physical Chemistry C* 112, 6729-6739.
- Gupta, V.K., Nayak, A. 2012 Cadmium removal and recovery from aqueous solutions by novel adsorbents prepared from orange peel and Fe₂O₃ nanoparticles. *Chemical Engineering Journal* 180, 81– 90.
- Hu, J., Chen, G.H., Lo, I.M.C. 2006 Selective removal of heavy metals from industrial wastewater using maghemite nanoparticle: Performance and mechanisms. *Journal of Environmental Engineering -ASCE*. 132, 709–715.
- Hua, M., Zhang, S., Pan, B., Zhang W., Lu L., Zhang Q. 2011 Heavy metal removal from water/wastewater by nanosized metal oxides: A review. *Journal of Hazardous Materials* 211(S1), 317-331.
- Kaur M., Singh M., Mukhopadhyay S. S., Singh D., Gupt M. 2015 Structural, magnetic and adsorptive properties of clay ferrite nanocomposite and its use for effective removal of Cr (VI) from water. *Journal of Alloys and Compounds*, 653, 202-211.
- Kikuchi, Y., Qian, Q.R., Machida, M., Tatsumoto, H. 2006 Effect of ZnO loading to activated carbon on Pb (II) adsorption from aqueous solution. *Carbon* 44, 195–202.
- Larachi F., Ihuta, I., Belkacemi, K. 2001 Catalytic wet air oxidation with a deactivating catalyst analysis of fixed and sparked three-phase reactors. *Catalysis Today*. 64(3-4), 309–320.
- Liu Y., Shan S., Yin J., Luo J., Zhong C. 2014 Characterization of magnetic NiFe nanoparticles with controlled bimetallic composition. *Journal of Alloys and Compounds* 587, 260-266.
- Najafi, M., Yousefi, Y., Rafati, A.A. 2011 Synthesis, characterization and adsorption studies of several heavy metal ions on amino-functionalized silica nano hollow sphere and silica gel. *Separation and Purification Technology* 85, 193-205.
- Nezamzadeh-Ejhih A., Kabiri-Samani M. 2013 Effective removal of Ni(II) from aqueous solutions by modification of nano particles of clinoptilolite with dimethylglyoxime. *Journal of Hazardous Materials* 260, 339– 349.
- Peng, S.H., Wang, W.X., Li, X.D., Yen, Y.F. 2004 Metal partitioning in river sediments measured by sequential extraction and biomimetic approaches. *Chemosphere* 57, 839–851.
- Sinkkonen, S., Rantion, T., Paasivirta, J., Peltonen, S., Vattulainen, A., Lammi, R. 1997 Chlorinated phenolic compound in coniferous needles. Effects of metal and paper industry and incineration. *Chemosphere* 35(6), 1175–1185.

- Su, Q., Pan, B.C., Wan, S.L., Zhang, W.M., Lv, L. 2010 Use of hydrous manganese dioxide as a potential sorbent for selective removal of lead, cadmium, and zinc ions from water. *Journal of Colloid and Interface Science* 349, 607–612.
- Tarasevich, Y.I., Klimova, G.M. 2001 Complex-forming adsorbents based on kaolinite, aluminium oxide and polyphosphates for the extraction and concentration of heavy metal ions from water solutions. *Applied Clay Science* 19, 95–101.
- Yuan, P., Liu, D., Fan, M., Yang, D., Zhu, R., Ge, F., Zhu, J. & He, H. 2010 Removal of hexavalent chromium [Cr(VI)] from aqueous solutions by the diatomite-supported/unsupported magnetite nanoparticles. *Journal of Hazardous Materials* 173, 614–621.
- Zhang, D., Zhang, C., Zhou, P. 2011 Preparation of porous nano-calcium titanate microspheres and its adsorption behavior for heavy metal ion in water. *Journal of Hazardous Materials* 186, 971–977.
- Zheng, Y., Yao, G., Cheng, Q., Yu, S., Liu, M., Gao, C. 2013 Positively charged thin-film composite hollow fiber nanofiltration membrane for the removal of cationic dyes through submerged filtration. *Desalination* 328, 42–50.
- Zhu, M., Lee, L., Wang, H., Wang, Z. 2007 Removal of an anionic dye by adsorption/precipitation processes using alkaline white mud. *Journal of Hazardous Materials* 149(3), 735-741.